Design, Fabrication, Testing and Validation of a Ruggedized Fiber Optic Sensing System (FOSS) for Launch Application

Allen R. Parker, Jr[1], Hon M. Chan[2] and Jonathan Lopez-Zepeda[3]
NASA Armstrong Flight Research Center, Edwards, California, 93523, U.S.A.

Paul A. Schallhorn[4]
NASA Kennedy Space Center, Merritt Island, Florida, 32899, U.S.A.

Fiber-optic sensors based on fiber Bragg grating (FBG) is desirable for structural health monitoring and is used for various aerospace applications such as measuring strain and temperature, where a single optical fiber can multiplex hundreds of FBG sensors. The National Aeronautics and Space Administration (NASA) Armstrong Flight Research Center (AFRC) (Edwards, California) has been developing an optical fiber-based sensing suite called Fiber Optics Sensing System (FOSS) over the past two decades. Successful strain monitoring flight demonstrations such as the NASA Ikhana (General Atomics, San Diego, California) remotely piloted aircraft and the X-56A Multi-Utility Technology Testbed (Lockheed Martin Corporation, Bethesda, Maryland) remotely piloted subscale aircraft have been performed. Interest in adapting fiber-optic sensors for aerospace applications has led to commissioning the development of a ruggedized FOSS system for spaceflight through the NASA Launch Services Program (LSP) at the NASA Kennedy Space Center (KSC) (Merritt Island, Florida).

In this paper, a ruggedized FOSS suitable for a launch environment is discussed in detail. Thermal analysis and enclosure design will be discussed as well as environmental testing such as shock, random vibration, thermal vacuum, and electromagnetic interference/electromagnetic compatibility (EMI/EMC). With all relevant environmental testing completed, a ruggedized FOSS unit has successfully passed all testing and is now deemed space-launch ready.

I. Nomenclature

α_{CTE} = *coefficient of thermal expansion*
α_n = *thermo-optics coefficient*
λ_b = *Bragg wavelength*
λ_0 = *initial Bragg wavelength of the Fiber Bragg Grating*
$\lambda_2, \lambda_3, \lambda_4, \lambda_n$ = *wavelength of laser*
λ_{FBG} = *resonant wavelength of fiber Bragg grating*
$\Delta\lambda_B$ = *change in Bragg wavelength*
ΔT = *change in temperature*
ε = *overall strain from mechanical and thermal effect*ε_m
n_e = *effective index of refraction*
Λ = *gap distance between each periodic refractive index change*
ρ_e = *strain-optic coefficient*

[1] Chief Engineer, FOSS, Advanced Systems Development Branch, NASA AFRC.
[2] Electronics Engineer, FOSS, Advanced Systems Development Branch, NASA AFRC
[3] Aerospace Engineer, FOSS, Advanced Systems Development Branch, NASA AFRC
[4] Project Manager, FOSS, VADR Technical Manager, NASA KSC

II. Introduction

As the aerospace community is transitioning to a reusable space-launch vehicle platform to support more frequent launches, this program optimized both costs and nondestructive evaluation (NDE) of aerospace structures, which is of paramount importance. Techniques used in NDE such as in situ structural health monitoring (SHM) can assess the health of an aircraft throughout its life cycle, for example, assessing potential failure modes after deployment. Fiber-optic-based sensing is attractive as part of the NDE suite since fiber-optic sensors could be integrated into the aircraft by either integrating the fiber sensors during the design process or prior to vehicle launch. Fiber-optic sensors based on fiber Bragg gratings (FBGs) are advantageous over conventional foil-type strain gages and include the ability to cascade multiple sensors into a single optical-fiber cable; therefore, reducing the number of cables required as well as reducing size, weight, and installation complexity. Another benefit of utilizing fiber sensors, as opposed to conventional gages and thermal couples, is that fiber sensors use optical light reflection as the sensing element; therefore, problems such as electrical arcing or electromagnetic interference (EMI) will not be a problem. This paper discusses a fiber-optic interrogator suite that is suitable for development of space flight applications.

The NASA Launch Services Program (LSP) at Kennedy Space Center is especially interested in this development effort for high-spatial-fidelity strain and temperature data applications – which the FOSS can provide – for structural health monitoring of space flight applications. The LSP commissioned a technology demonstration of a space-rated FOSS system to provide strain and temperature monitoring on a launch vehicle. As part of an avionics unit on the NASA Space Technology Mission Directorate Low-Earth Orbit Flight Test of an Inflatable Decelerator (LOFTID), this effort led to the development of a ruggedized FOSS unit that was on board the vehicle to monitor rigid aeroshell re-entry temperature and assess the effectiveness of the inflatable heat shield to protect a large payload [1].

An introduction to optical frequency domain reflectometry (OFDR) deployment at NASA will be discussed, then the baseline FOSS hardware and software that has been developed and deployed will be summarized. The design and fabrication of a ruggedized version of the FOSS avionics unit will also be presented, followed by multiple environmental tests, resulting in a space-rated FOSS system that is now ready and is available to support future launch applications.

III. Principle of Optical Frequency Domain Refractometry

Fiber optic-based sensing has the advantage to cascade multiplex sensors onto a single telecommunication-based fiber, whereas other NDE electronic-based sensors (such as resistive foil gage or thermocouple) use point measurements, where multiple wires are needed and routed throughout the aerostructure in order to conduct measurements, adding weight and complexity to deployment. The NASA has been researching using fiber-optic-based sensing for structural health monitoring [2, 3], and many experimental results have shown that results from fiber sensors - especially based on fiber Bragg gratings - are comparable to traditional strain gage or thermal couple sensors [4-6].

Fiber Bragg gratings are fabricated with periodic changes to the index of refraction, which occur in the core of the optical fiber. These changes of refraction, accumulated together, have led to the reflection of the resonant wavelength of the grating. Equation (1) shows the resonant wavelength of any FBG grating:

$$\lambda_{FBG} = 2n_e\Lambda \tag{1}$$

where λ_{FBG} is the design wavelength of each FBG; ne is the effective index of refraction change in the single-mode fiber; and Λ is the gap between each periodic refractive index change. To fabricate these changes in the index of refraction, the fiber will be exposed to an ultraviolet (UV) laser light with a "zebra pattern" phase mask to produce the desired resonant wavelength.

When exposed to environmental perturbations such as mechanical strain or temperature change, a change in the pitch size Λ of said grating was observed, which causes changes in both coefficient of thermal expansion (CTE) and strain-optics coefficient [7]. Equation 2 shows the resulting wavelength shift:

$$\frac{\Delta\lambda_B}{\lambda_0} = (1-\rho_e)\varepsilon + \alpha_n\Delta T \tag{2}$$

where $\Delta\lambda_B = (\lambda_B - \lambda_0)$ is the delta change in Bragg wavelength caused by environmental change; λ_0 is the initial Bragg wavelength of the FBG; ρ_e is the strain-optic coefficient (constant) of the FBG; $\varepsilon = \varepsilon_m + \alpha_{CTE}\Delta T$ is the overall strain based on the amount of length being stretched or compressed, either via mechanical strain (ε_m) or through coefficient of thermal expansion (CTE); and α_{CTE} and α_n are the coefficient of thermal expansion and thermo-optic

coefficient of the fiber core at room temperature, respectively. By monitoring the shift of each FBG wavelength, either the strain or temperature of the environment can be measured.

There are two common methods to interrogate FBGs. The first method utilizes wavelength division multiplexing (WDM), which involves reading the reflection value of each resonant wavelength grating as it is being shifted, where each FBG will have a unique resonant wavelength (usually separated by 5 nm) to prevent overlapping in the event that one grating is pulled while another one is compressed. A typical WDM system is shown in Fig 1. A WDM-based interrogator is usually powered by a broadband incoherent light source, and the reflected light from each FBG is collected via a bulk optic-based grating. The interrogation speed of the mentioned spectrum analyzer is dependent on the refresh rate of the charge-coupled device (CCD) camera, and the bandwidth resolution is based on the number of CCD arrays available on the chipset as well as the reflecting distance from the diffraction grating. Typically, the resolution from a commercial broadband light-source-based WDM interrogator ranges up to approximately 1 picometer (pm); however, the trade-off for a detector-based WDM system hedges on the reliability of the bulk optical components, specifically, on the deflection grating, where optical alignment problems caused by vibration can render inaccurate results from the system.

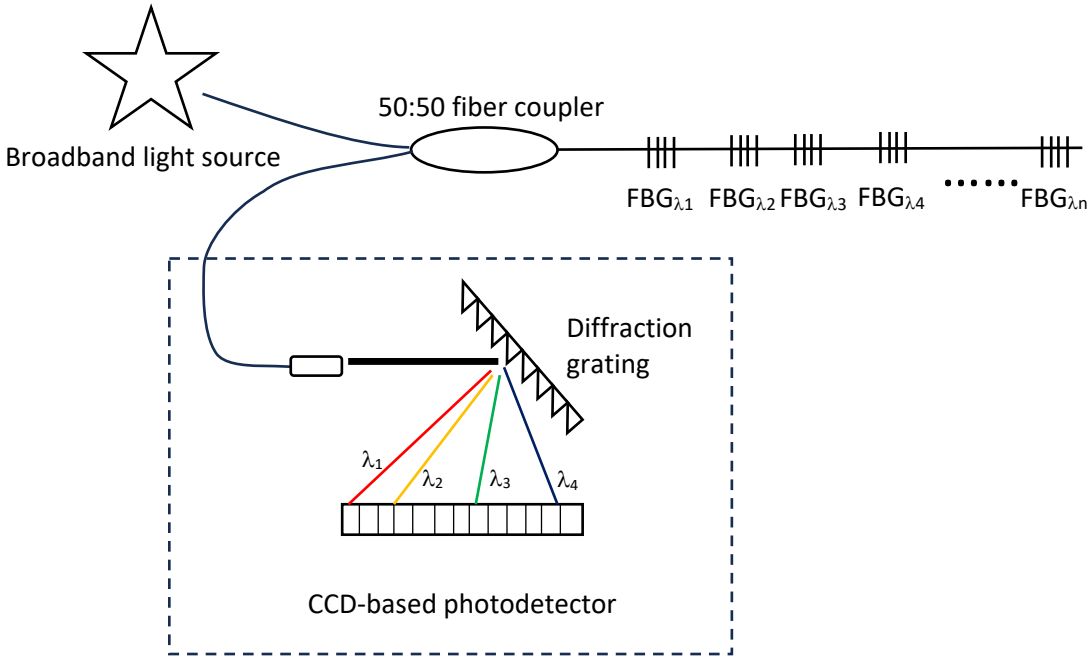

Fig. 1 A typical WDM-based interrogator setup via a spectrum analyzer (dotted line), composed from a fiber collimator; a diffraction grating that separates each unique wavelength from each FBG; and a CCD-based photodetector to read the wavelength from each FBG sensor.

The second method of interrogating FBGs utilizes optical frequency domain reflectometry (OFDR) [8], which enables the measurement of hundreds of FBGs in a single fiber, where the bandwidth limitation for WDM-based measurement techniques is eliminated. Details of OFDR operation have been discussed elsewhere [9]. In summary, OFDR techniques use very low reflectivity (less than 0.01 percent) gratings written in the same wavelength, which enables cascading of hundreds of gratings into a single fiber with little signal loss. By tracking wavelength change in each individual grating via signal processing, the strain or temperature change of that grating can be retrieved. Figures 2a) and 2b) show the optical network difference between WDM- and OFDR-based platforms.

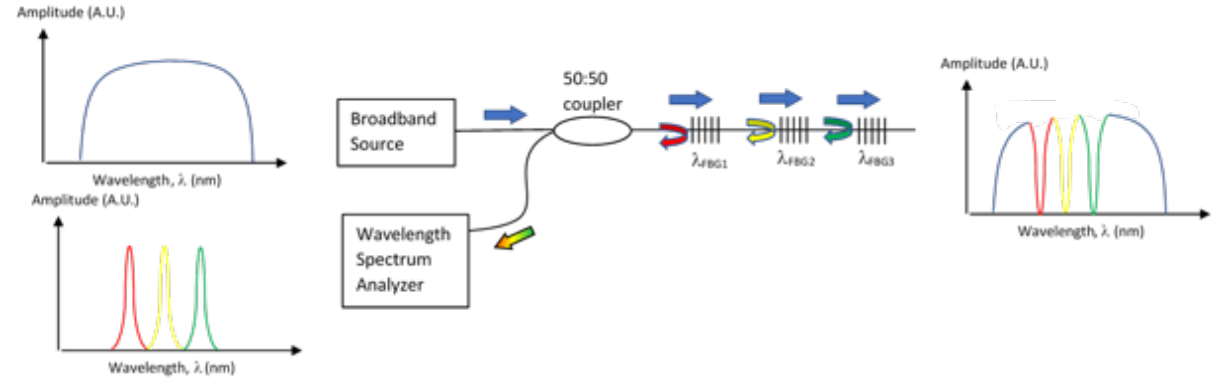

a)

Fig. 2a) Graphical representation of WDM.

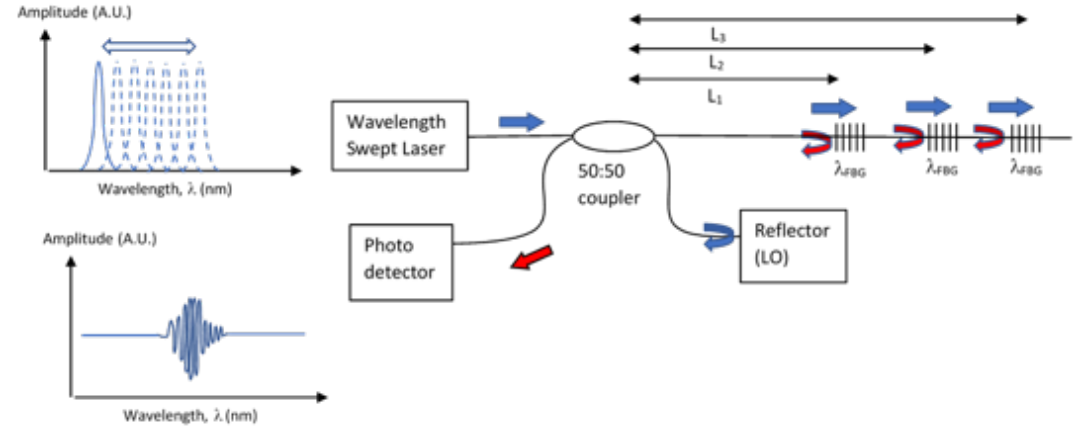

b)

Fig. 2b) The OFDR FBG sensing scheme.

The WDM-based sensing, as shown in Fig. 2a), is directly measuring the reflective wavelengths of all the FBGs, each having a unique center wavelength, available within the fiber. A challenge of WDM-based sensors is the potential for grating-to-grating aliasing, wherein measurement uncertainty can occur when the center wavelength of one sensor overlaps with an adjacent sensor. The OFDR, as shown in Fig. 2b), is based on interference measurement. Despite each FBG utilizing OFDR, each having the same center wavelength, the difference in location causes a unique beat frequency that can be identified using Fourier domain transformation.

IV. Fiber-Optic Sensing Overview

The NASA fiber optic sensing system (FOSS) is a complete suite that consists of a system-in-a-box hardware interrogator unit, as shown in Fig. 3. The FOSS includes the integrated hardware, which contains a continuously tuned wavelength-swept laser; a custom optical network that can simultaneously sample multiple channels of fiber sensor arrays in real time; and generates a real-time reference clock. A custom field-programmable gate array (FPGA) chipset runs a custom algorithm to facilitate a Fast Fourier Transform/inverse Fast Fourier Transform (FFT/iFFT) calculation process. A general-purpose central processing unit (CPU) acts as a server for data storage and data transport; the CPU conducts background tasks such as network transfer of real-time data, using Ethernet connectivity, to multiple clients.

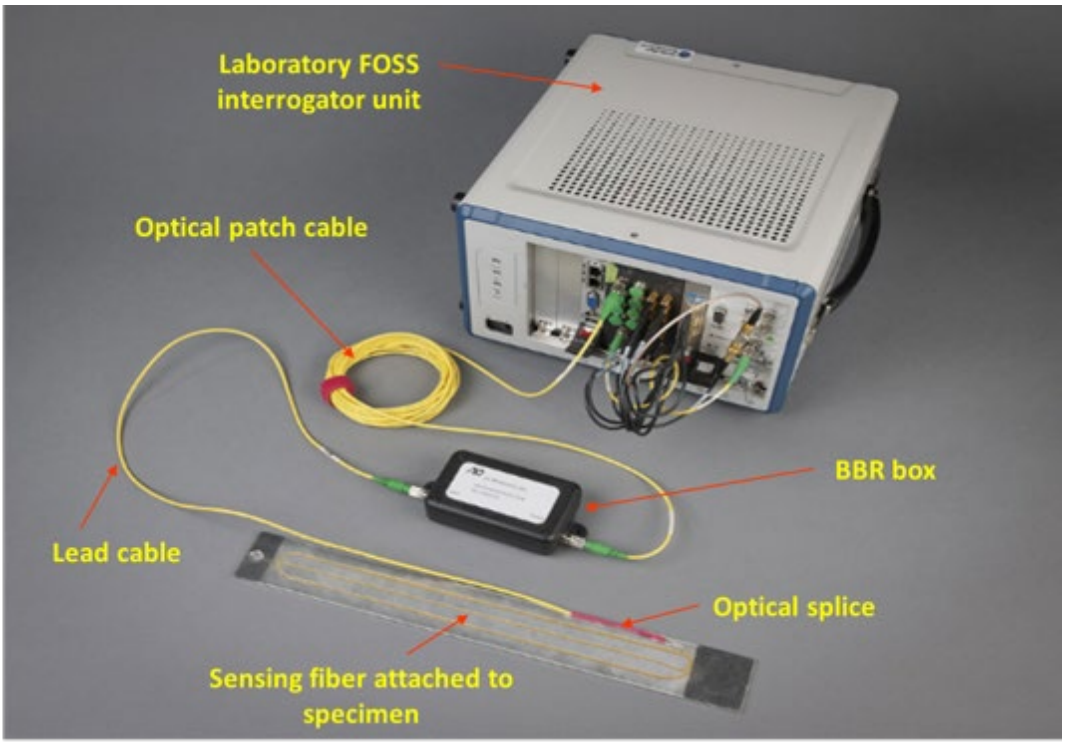

Fig. 3 The FOSS is comprised of a system-in-a-box hardware interrogator unit as well as an optical-fiber sensing array, consisting of multiple low-reflectivity FBGs, each having the same center wavelength.

Fiber grating array sensors, composed of many FBGs with low reflectivity, are utilized for OFDR sensing. Typical FBG sensors utilized in the WDM scheme have a high-reflectivity value (>50 percent) so that each center wavelength sensor can be identified; however, in OFDR application, each FBG sensor has the same center wavelength as well as a much lower reflectivity (0.01 to 0.001 percent) than typical FBG sensors. As a result, hundreds of identical sensors can be in the same fiber without incurring significant light loss. In FOSS application, each sensing array can be composed of up to 40 ft of low reflectivity gratings connected to an optical interferometer box or a broadband reflector (BBR). The BBR contains the local oscillator (LO) arm that marks the beginning distance calculation for each of the sensors. A fiber patch cable, up to 100-ft long, is connected from the FOSS interrogator box to the BBR box so that the interrogator can be located a long distance away from the sensing, which is beneficial in combustible or EMI-susceptible environments.

V. FOSS for Ruggedized Environment

The NASA Armstrong Flight Research Center (AFRC) (Edwards, California); NASA Human Exploration and Operations (HEO) committee; NASA Langley Research Center (LaRC) (Hampton, Virginia) and the NASA Launch Services Program (LSP) all collaborated to develop, test, and flight-demonstrate a space-rated FOSS, where four identical units were fabricated, built-out, and tested. One unit serves as the qualification unit and one unit was used to support the LOFTID flight.

For FOSS to be operational under the requirements of LOFTID, the motto of “do no harm” to the payload is executed; therefore, the FOSS space-ready unit is designed with the following guiding principles:

1) Prevent the high-voltage rail of 150 V within FOSS to unexpectedly arc in a vacuum space environment, therefore the enclosure is pressurized with nitrogen gas at 1 atm;
2) Provide for the enclosure to be maintained at atmosphere pressure; the enclosure walls must be able to maintain pressure without buckling in a vacuum space but also act as a heat-sink for conduction cooling; and
3) Ensure that the laser within FOSS can survive vibration and shock requirements associated with rocket launch and stage separation by using specially designed shock mounts; however, because the laser is now staged on top of the shock mounts, a custom-made thermal strap was fabricated to facilitate cooling.

By satisfying these requirements, a blueprint for the FOSS unit for a space environment was designed. Table 1 shows the technical specification of the FOSS launch system, located within the project design review. The FOSS unit

has four unique optical channels, with each optical channel able to interrogate up to 40 ft of fiber sensors. Since the spatial resolution for each sensor is one-half inch, it is possible to put in up to 960 sensors within a single optical channel; therefore, in total, more than 3,800 sensors can be interrogated simultaneously, providing that all four optical channels are occupied.

Table 1 Launch Capable FOSS Specifications.

Launch Capable FOSS Specifications	
Parameters	**Units**
Fiber channel count	4
Max sensing fiber length	40 ft
Max patch cable length from system	≈100 ft
Fiber type	Single-mode fiber (SMF)-28
Max no. of sensors/fibers	2,000
Max Sample rate	50 Hz
Onboard storage	32 GB
Interface	Gigabit Ethernet
User Interface Protocol	transmission control protocol (TCP)/internet protocol (IP)
Operational Communication Protocol	user datagram protocol (UDP)
Power	70 W at 28 VDC
Weight (including enclosure)	38 lbs
Size (application specific)	18.15 in by 8.625 in by 6.25 in

Figure 4 shows a ruggedized four-port optical channel FOSS interrogator suite component, which is composed of four Diamond (Diamond SA, Losone, Switzerland) hermetically sealed fiber-optic connectors. Located within the ruggedized aluminum enclosure are the following: a wavelength tunable laser, optical network, photodetector, data processing unit, and solid-state memory storage. The enclosure is 18.15-in deep by 8.625-in wide by 6.25-in tall and weighs approximately 34 lb. Figure 5 shows a drawing denoting the overall box dimensions.

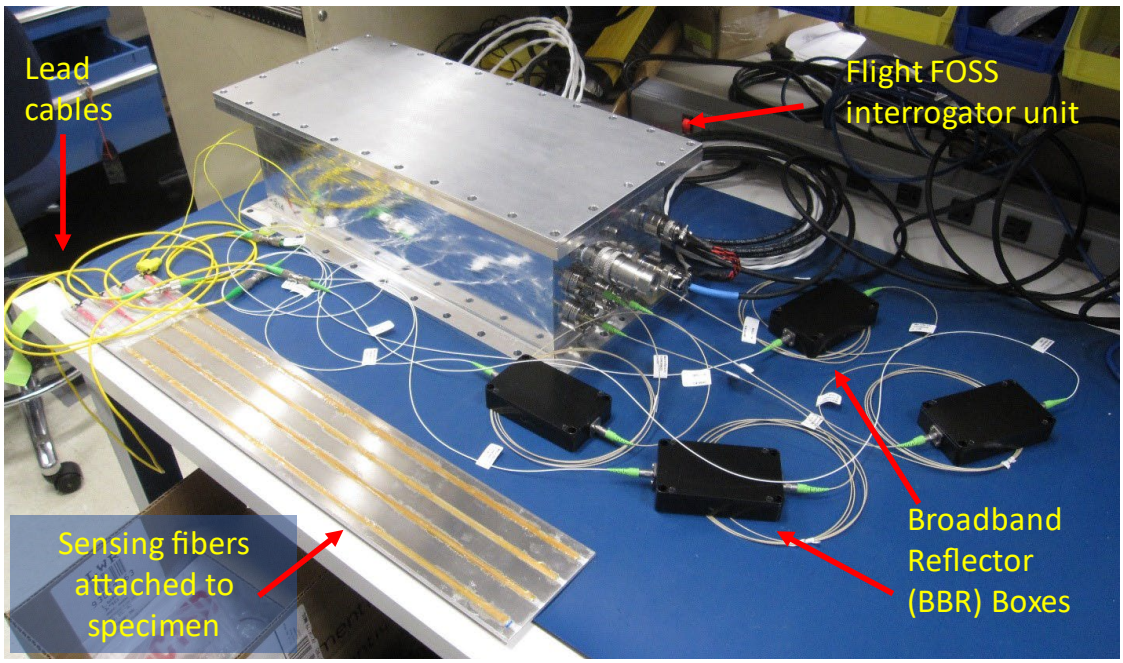

Fig. 4 Ruggedized four-port FOSS interrogator suite with BBR boxes.

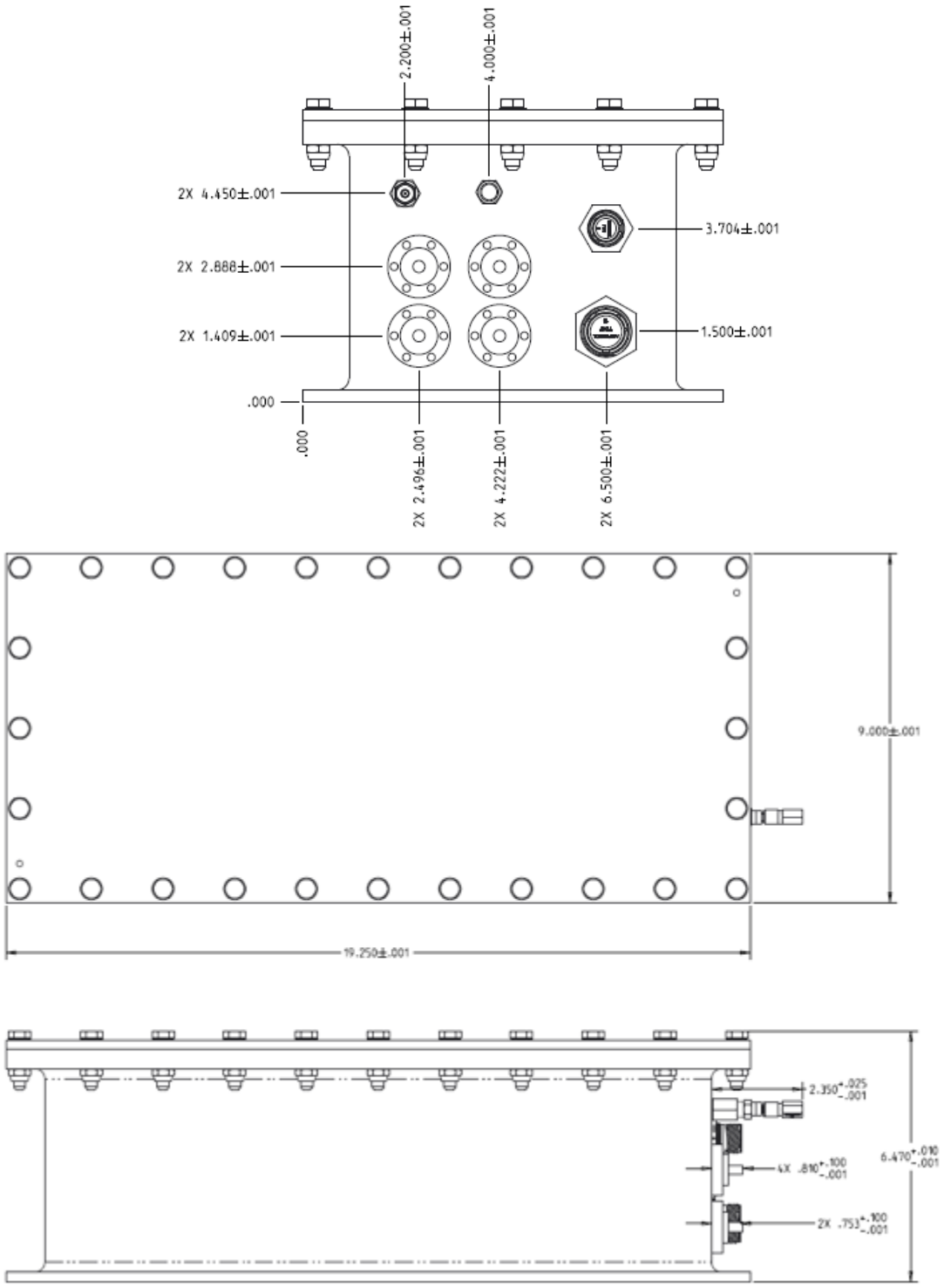

Fig. 5 Engineering drawing showing FOSS dimensions.

The FOSS unit has multiple input and output ports consisting of electrical, optical, and pneumatic components. The unit has two electrical connections - power and communication - located on the front face of the box. Power to the unit will be supplied by the launch vehicle via 28 VDC, at 8 A, with an acceptable voltage drift tolerance between

19 and 32 VDC. The nominal operating current for the unit is 2.4 A, with a peak inrush current 8 A, over a time period of 10 ms.

The FOSS unit communicates through a custom hermetically sealed Diamond Midi AVIM® connector, where the interface provides Ethernet connection up to a 1,000-MB speed via either user datagram protocol (UDP) or transmission control protocol (TCP) to other network-attached devices. The two pneumatic ports are for filling or draining the hermetically sealed interior of the unit, respectively. The unit can be pressurized up to 20 psig before the relief valve is activated to maintain its interior pressure.

VI. Environmental Testing Protocol to Certify FOSS for Flight

To certify FOSS for flight, test plans were established. One flight unit would be subjected to environmental testing at qualification level while all other flight units would be subjected to testing under acceptance level. The purpose of the test plans was to ensure fulfillment of the test verification requirements. Figure 6 showcases the integration and test (I&T) program that the FOSS system is subjected to. First, to ensure that the units are functional, a functional test is conducted, a baseline is established, and a mass properties test is conducted. Next, an initial series of EMC/EMI tests were performed. Then, shock, vibration, thermal cycle, thermal vacuum, and finally, a second set of EMC/EMI tests were performed, respectively. The test protocol is followed after each set of tests, ensuring that the box does not break any baseline configuration in order to validate subsequent tests. Test parameters are based on Space and Missile Systems Center Standards (SMC Standard SMC-S-016) test requirements for launch, upper-stage, and space vehicles.

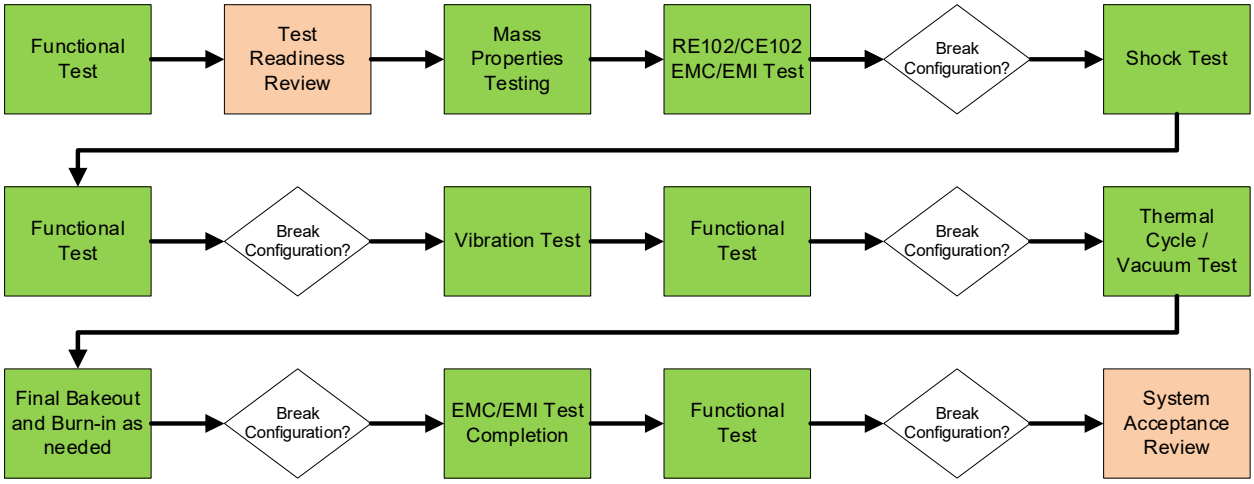

Fig. 6 General FOSS I&T workflow.

A series of pyroshock testing was conducted at MGA Research Corporation in Manassas, Virginia (MGA Research Corporation, Akron, New York), from September 2020 to April 2022, and followed the requirements for a shock environment suitable for a launch environment. The FOSS qualification unit has undergone several series of shock tests (as shown in Table 2) attributable to the optical network design limitations, which were brought about by a series of shock events. Overall parts of the subsystem saw 22 shock events, where a typical shock qualification (per SMC-S-016) consisted of a series of nine shock tests. At the end of all the shock testing events, all subsystem components survived at least nine shock events, three shock events per x, y, and z axes, respectively. As a result of time constraints, however, the CPU carrier board from the qualification unit was damaged after 22 shock events but was later replaced for performance vibration testing. Figures 7-9 show the shock testing in x-, y-, and z-axes configurations, respectively, with modification of the test fixture to reduce the moment arm seen by the unit during testing.

Table 2. Shock testing summary for a FOSS-qualified unit that shows each shock test design system revision leading up to eventual shock testing acceptance.

Shock Test	# Shocks in Each Direction			Components	Results
	X	Y	Z		
1st	3	0	0	Full system test	Optical network failure. Mounts replaced after test.
Optical Network	3	3	3	Subcomponent test	Fully operational through all shocks. Component passed.
2nd	3	3	3	Full system test	Optical network failure. Completed remaining axis. Rest of system was operational after 9 shocks.
BBR	3	3	3	Subcomponent test	All three directions tested at once. Result Pass
Delta Qual	4	3	3	Full system test	Carrier board short on shock 7 during testing. Rest of system was operational after 10 shocks.

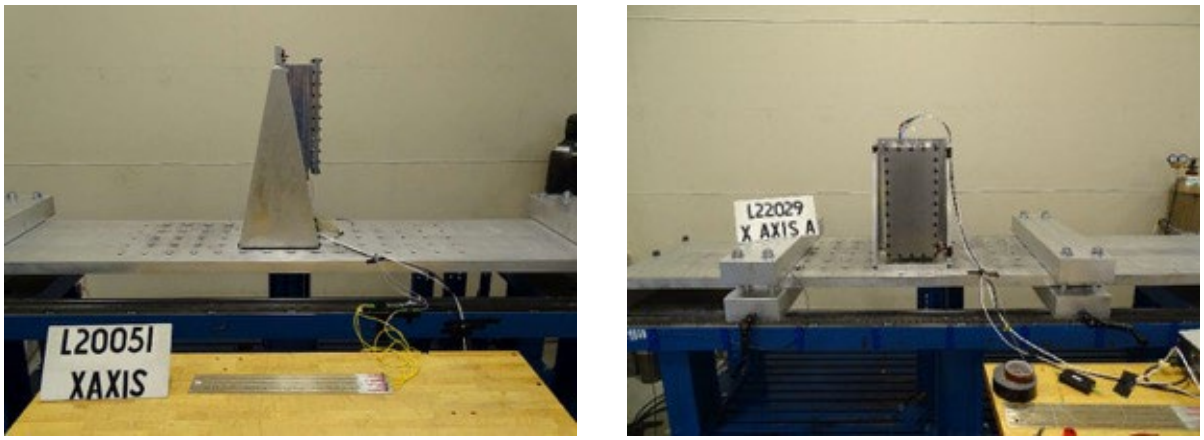

a) **b)**

Fig. 7a) First set of X-axis shock testing; and Fig. 7b) Delta Qual Shock testing with the test fixture removed to reduce the moment arm associated with increased shock effect.

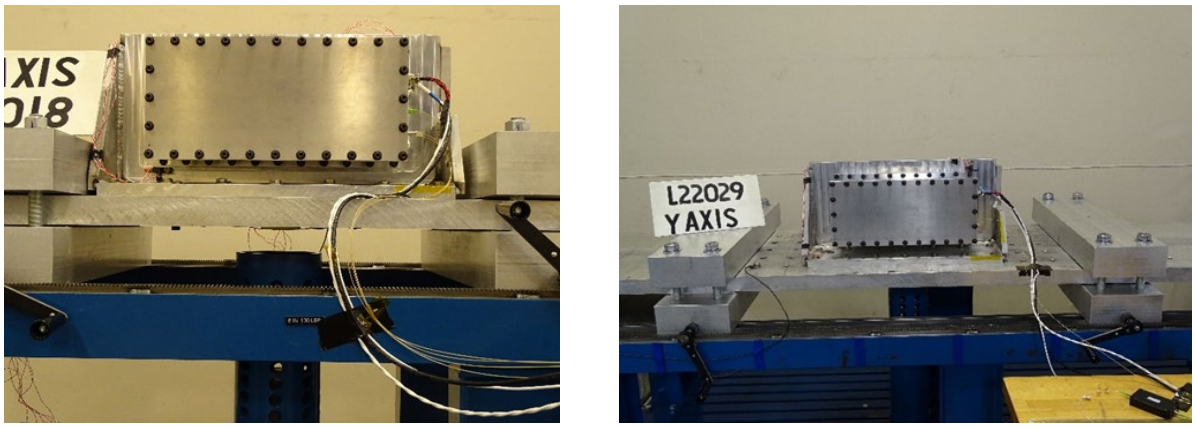

a) **b)**

Fig. 8a) First set of Y-axis shock testing; and Fig 8b) Delta Qual of Y-axis shock testing.

a)

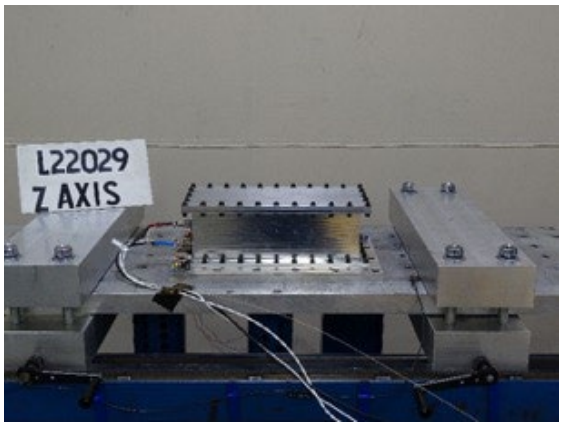

b)

Fig. 9a) First set of Z-axis shock testing; and Fig. 9b) Delta Qual of Z-axis shock testing.

Qualification level of random vibration testing was conducted at AFRC in July 2022. There were three FOSS units available for random vibration testing. There was a qualification level as well as a maximum predicted environment (MPE). As defined in SMC-S–016A, proto-qualification level is defined as 3 dB above the envelope of MPE and able to survive a minimum time duration of 2 min in each orthogonal direction. The FOSS qualification unit failed its qualification test because the swept-source laser, after enduring 22 shock events, failed at the maximum level of vibration testing. Two other FOSS units were selected to continue testing via the proto-acceptance level and both passed testing. Figures 10-12 show the FOSS pro-qualifying unit undergoing random vibration testing in x-, y-, and z-axes configurations, respectively.

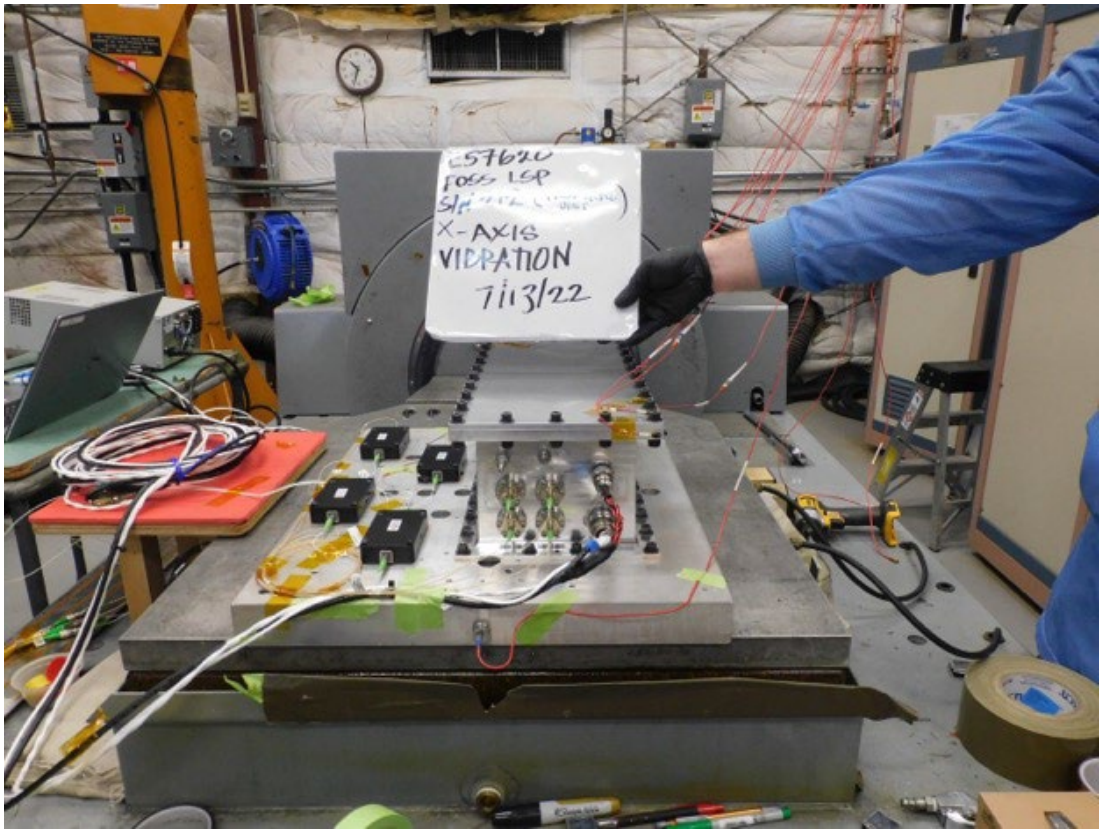

a)

Fig. 10a) X-axis random vibration testing.

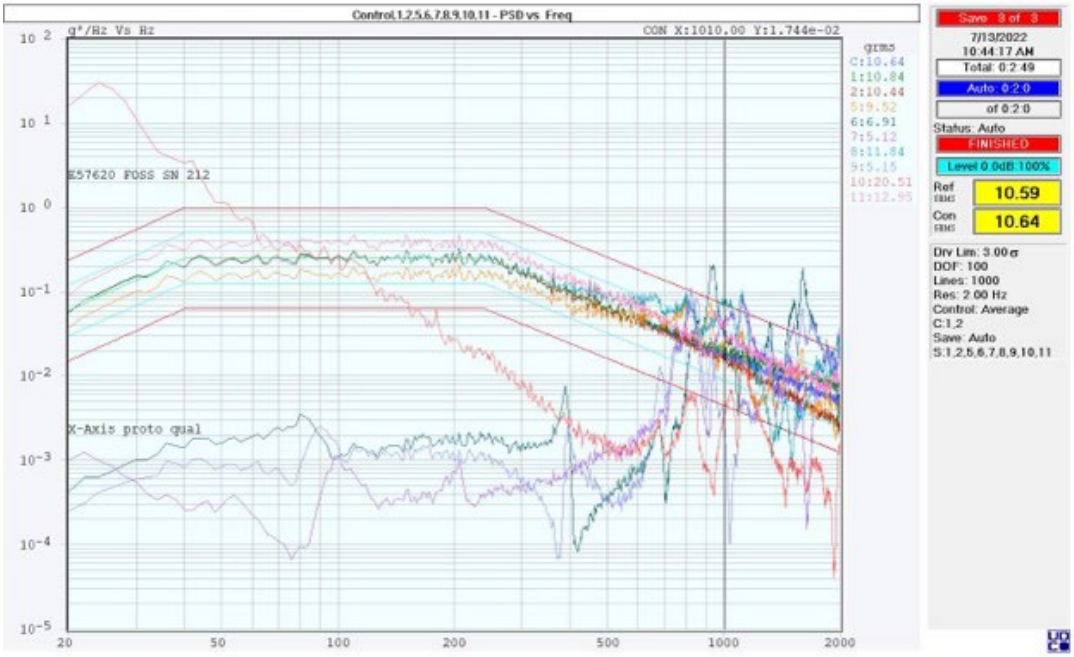

b)

Fig. 10b) Proto-qualification random vibration testing on FOSS unit (serial number 212). The accelerometers are within 3 dB above the envelope of the MPE+3 dB, within a minimum time duration of 2 min.

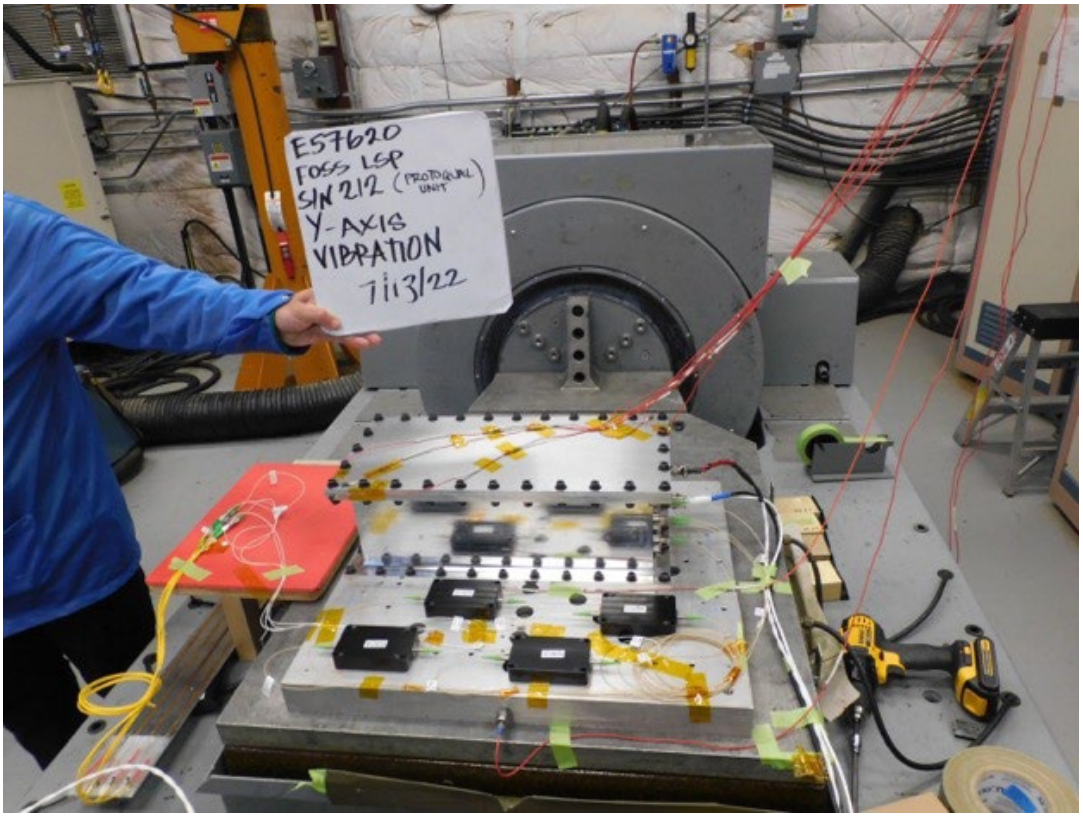

a)

Fig. 11a) Y-axis random vibration testing.

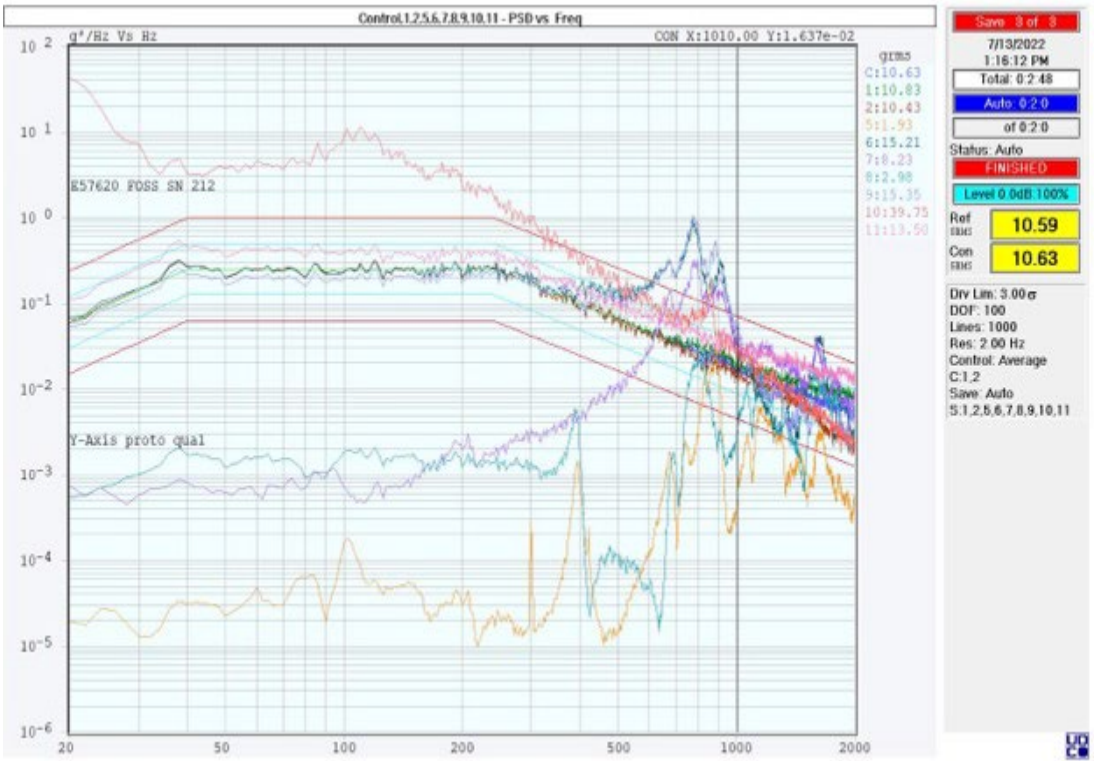

b)

Fig. 11b) Proto-qualification random vibration testing on FOSS unit (serial number 212). The accelerometers are within the envelope of MPE+3 dB, within a minimum time duration of 2 min.

a)

Fig. 12a) Y-axis random vibration testing.

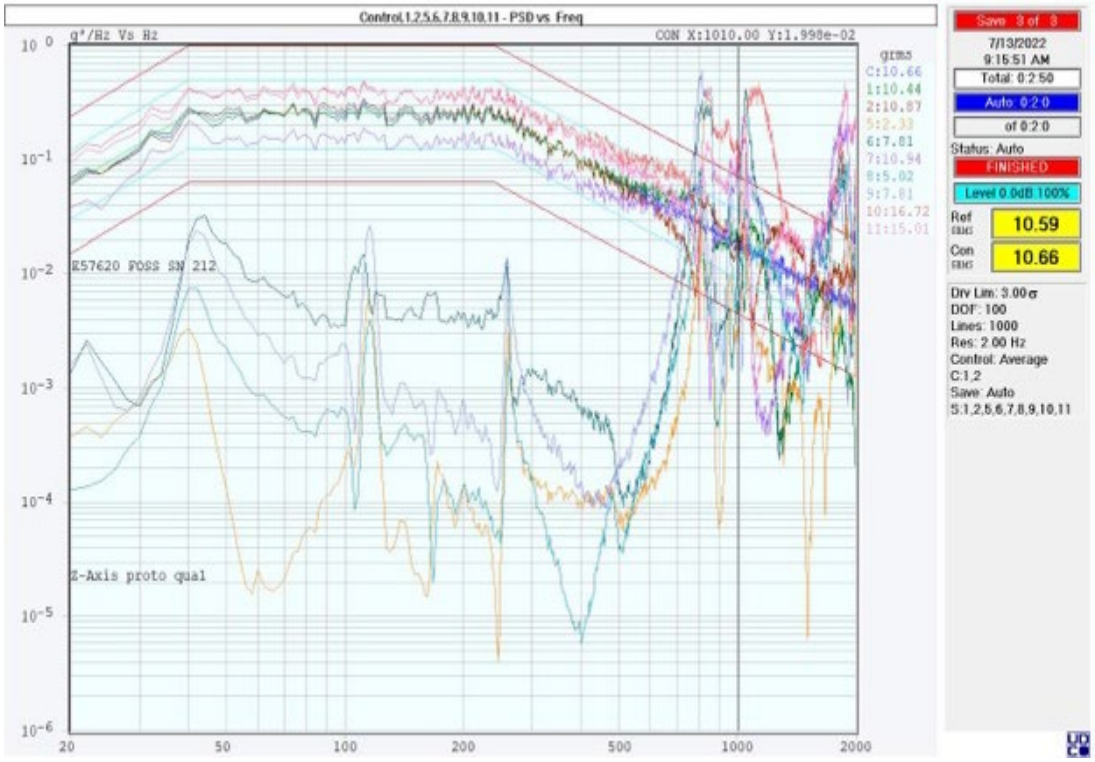

b)

Fig. 12b) Proto-qualification random vibration testing on FOSS unit (serial number 212). The accelerometers are within the envelope of MPE+3 dB, within a minimum time duration of 2 min.

Proto-Qualification thermal cycling of FOSS units was conducted at KSC from August 10-17, 2022. The boxes endured different temperature exposures (ranging from extreme hot to extreme cold) to ensure all components of the FOSS unit were still functional after thermal cycling. Overall, 16 hot and cold cycles were run continuously, over the course of seven days, with the temperature profiles shown in Figs. 13-15. Since the swept-source laser has a lower tolerance with respect to the rest of the electronic stacks of the unit, there was an aliveness test to ensure that all FOSS electronics were running accurately, without the laser turning on during testing. Additionally, laser functionality tests were run at a more intermediate temperature. One of the proto-qualified FOSS unit lasers, however, did fail during testing; therefore, only one unit (serial number 212) successfully completed all testing. Figure 16 shows the FOSS units residing in the thermal chamber.

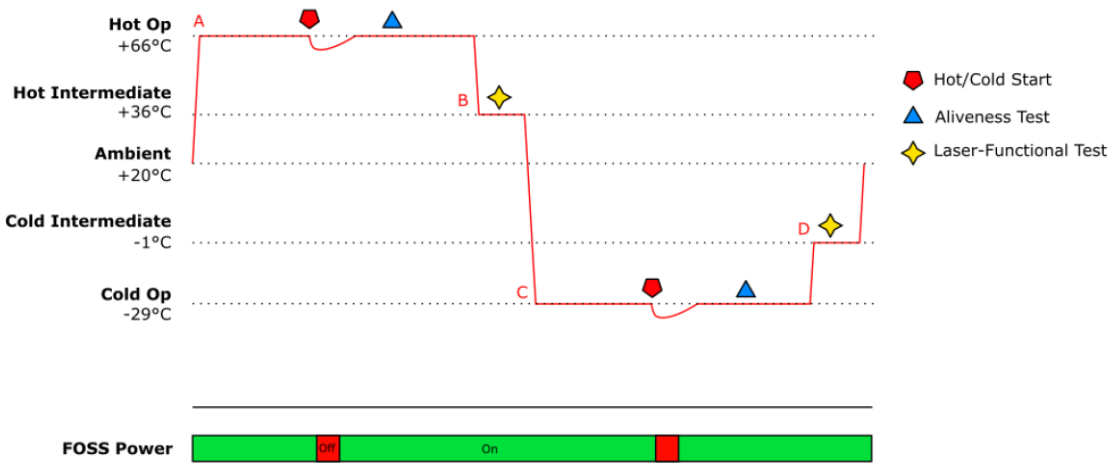

Legend:

Plateau	Temperature	Plateau Duration	Tests
A	66 ºC ±3 ºC	270 min	FOSS Aliveness
B	36 ºC ±3 ºC	120 min	FOSS Functional
C	-29 ºC ±3 ºC	270 min	FOSS Aliveness
D	36 ºC ±3 ºC	120 min	FOSS Functional

Fig. 13 Thermal cycling proto-qualification temperature profile (Cycles 1 & 16).

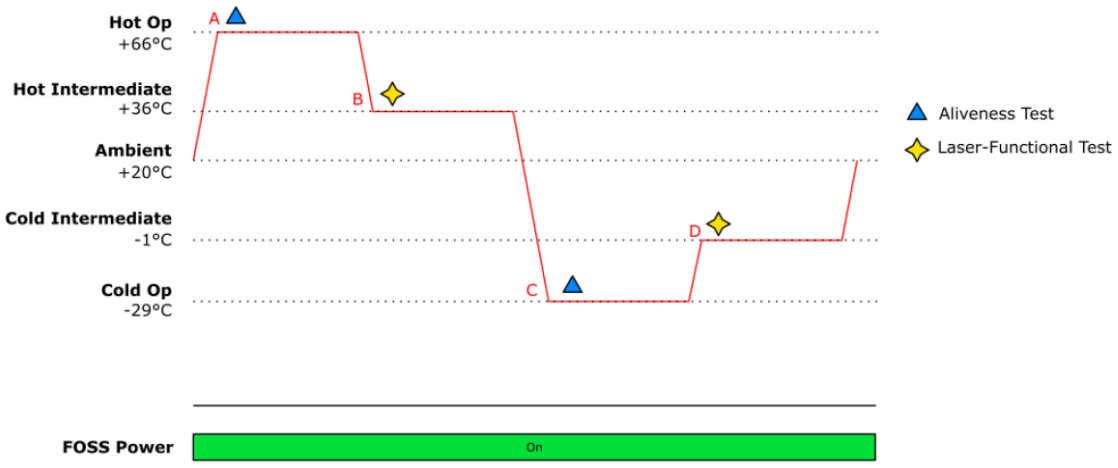

Legend:

Plateau	Temperature	Plateau Duration	Tests
A	66 ºC ±3 ºC	120 min	FOSS Aliveness
B	36 ºC ±3 ºC	120 min	FOSS Functional
C	-29 ºC ±3 ºC	120 min	FOSS Aliveness
D	36 ºC ±3 ºC	120 min	FOSS Functional

Fig. 14 Thermal cycling proto-qualification temperature profile (Cycles 2-15).

Fig. 15 FOSS units inside a thermal chamber prior to undergoing thermal cycling at NASA KSC.

Proto-qualification thermal vacuum cycling of a FOSS unit was conducted at LaRC from September 12-15, 2022. Figure 17 shows the FOSS unit inside the thermal vacuum chamber. The unit was subjected to hot and cold temperature cycles, similar to the thermal cycle testing profile, previously shown in Figs. 13-14, but also under a vacuum conduction less than 1 x 10^{-4} Torr, with a temperature transition between 3- to 5-deg C. Overall, four hot and cold thermal vacuum cycles were continuously run. Ultimately, the FOSS unit passed all thermal-vacuum cycle testing without any problems. An analysis of the thermal data led to the conclusion that FOSS met the requirements and demonstrated the ability to function properly under low and high temperatures, and the equipment is sufficiently capable to operate in a launch vehicle environment.

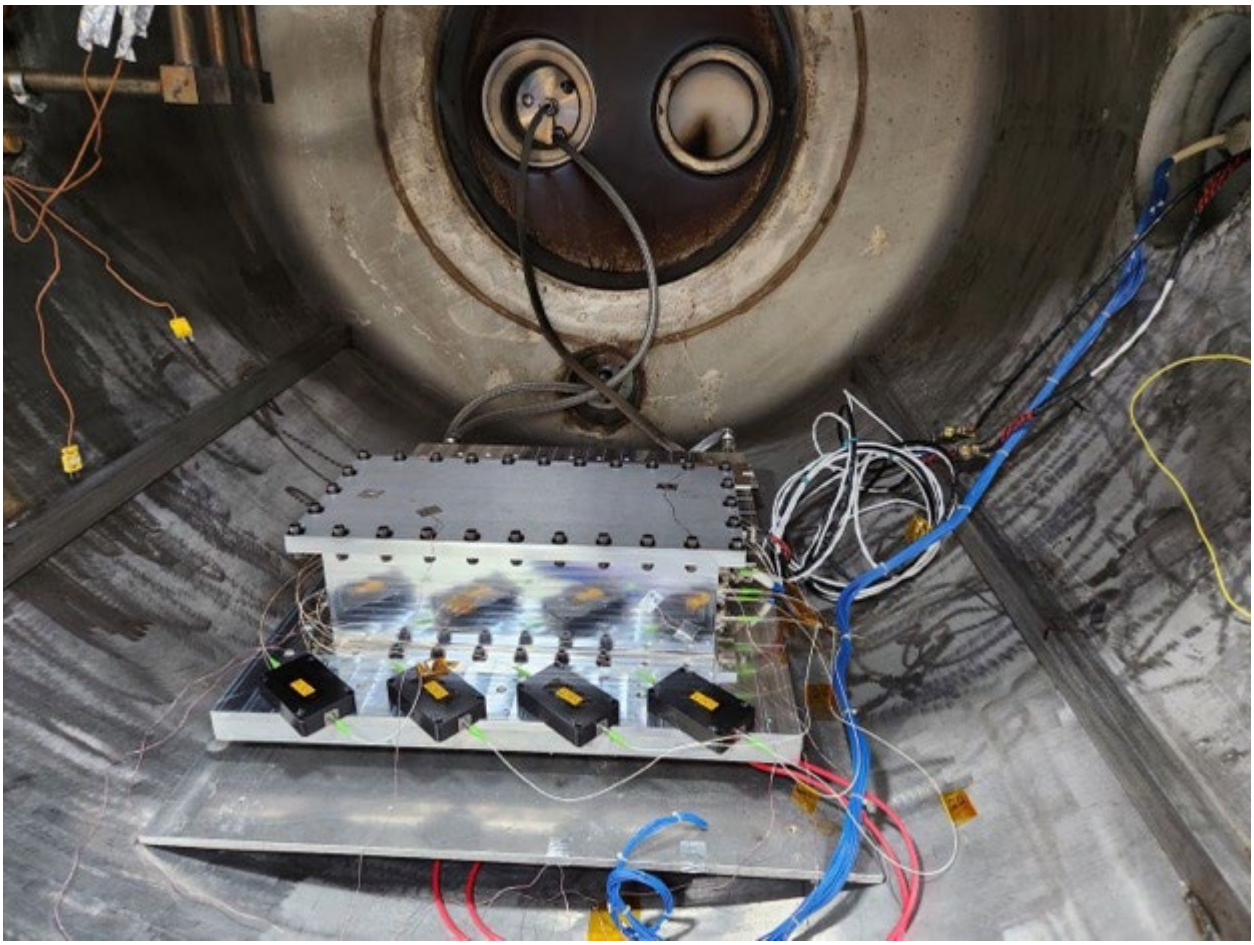

Fig. 16 FOSS unit undergoing thermal vacuum chamber testing at NASA LaRC.

Proto-qualification of EMI/EMC testing was conducted at LaRC from October 17-20, 2022. The testing assessed FOSS radiated and conducted emission (CE) profiles. These tests are listed on SMC-S-008. The testing included CE tests as well as radiated emissions (RE) tests. Figures 17 and 19 show the FOSS unit undergoing various EMI/EMC testing, and Figs. 18 and 20 show the results of the testing, where the FOSS unit radiates below the required threshold. The outcome of this testing concluded that the current FOSS design is expected to perform to its full array of intended functions without causing electromagnetic disturbances that could interfere other avionics equipment.

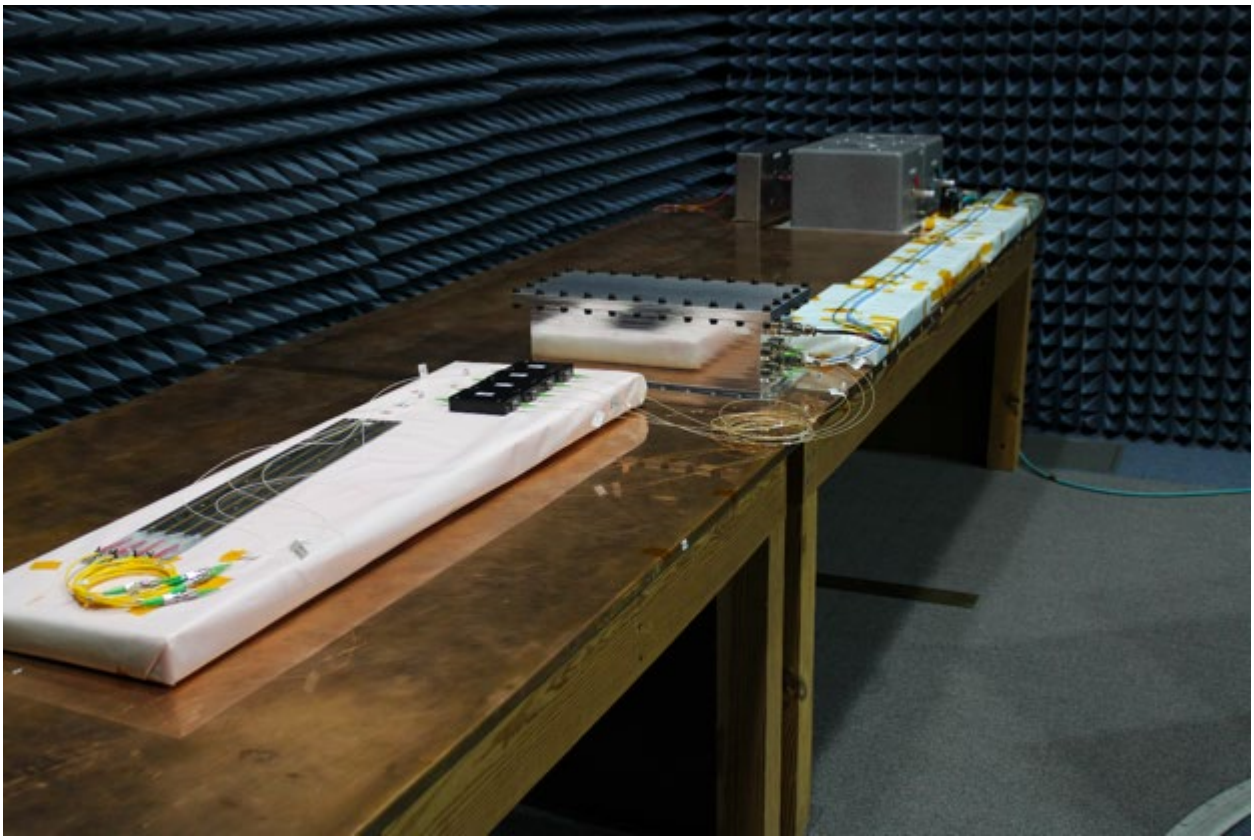

Fig. 17 FOSS undergoing EMI/EMC testing.

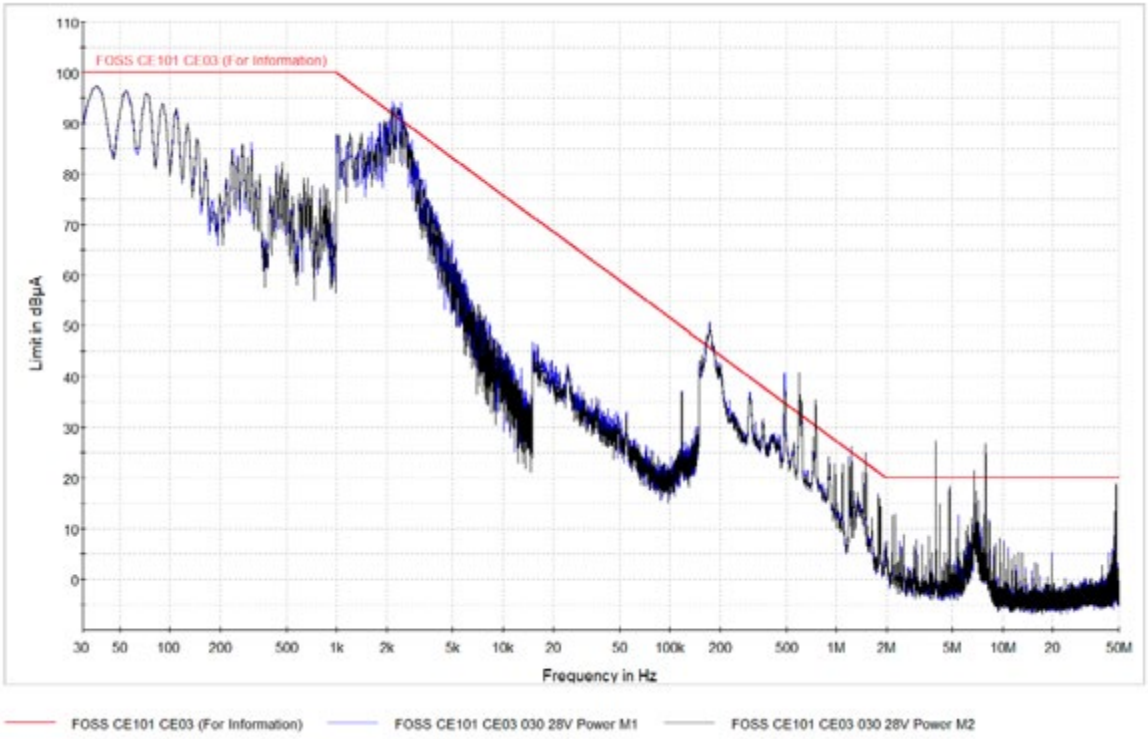

Fig. 18 FOSS undergoing EMI/EMC testing under CE 101 and within a range of 3010k Hz.

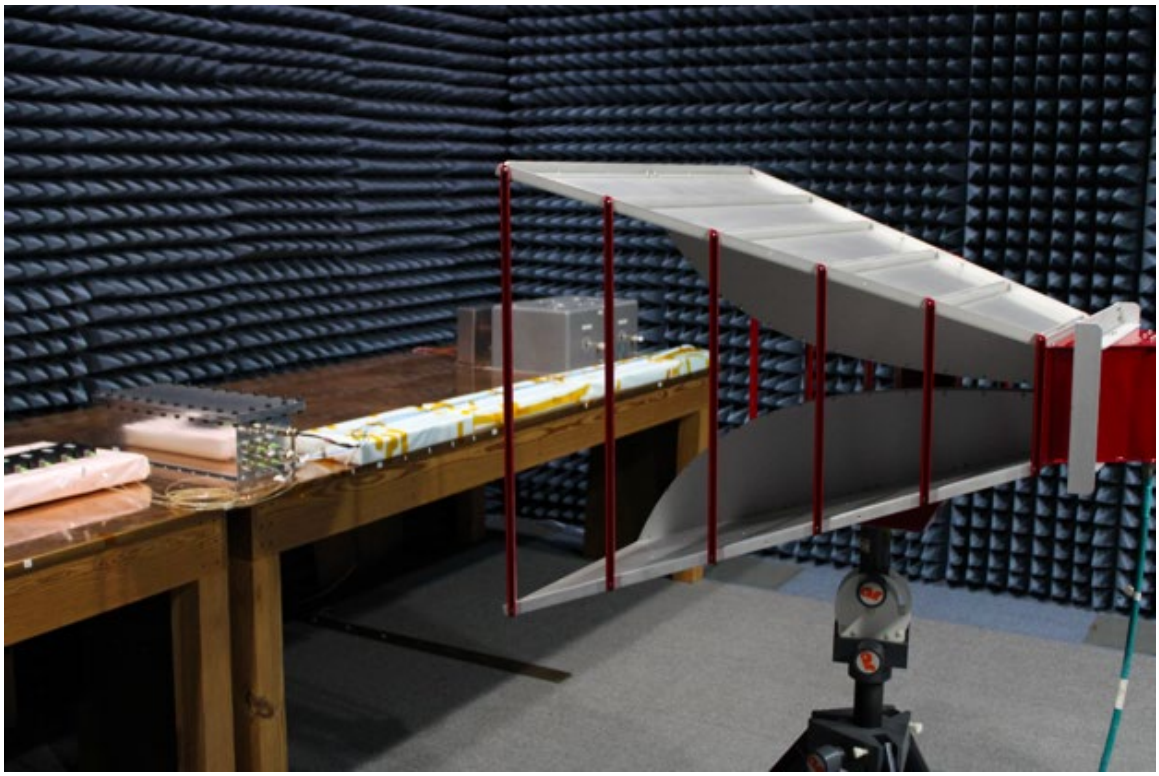

Fig. 19 FOSS undergoing RE 102 testing within a range of 200 MHz-1 GHz.

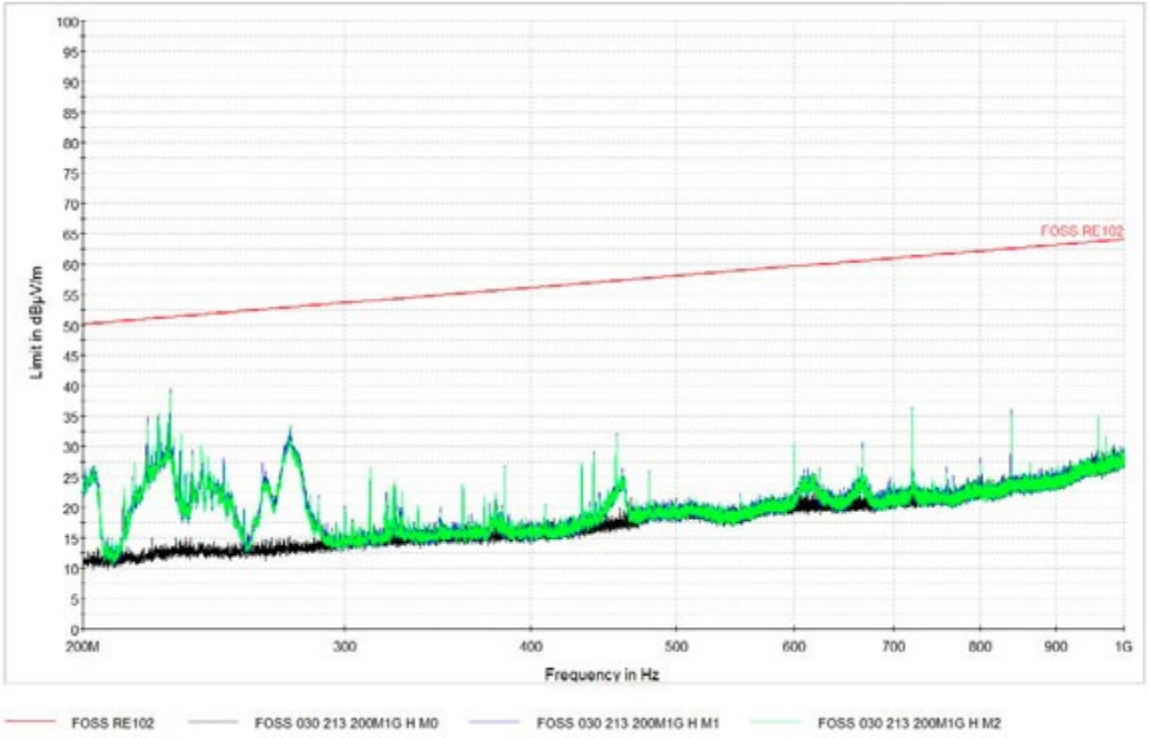

Fig. 20 FOSS RE 102 testing within a range of 200 MHz-1 GHz.

Conclusion

With the potential of multiplexing multiple sensors onto a single optical fiber and immunity from EMI interference, the NASA Fiber Optic Sensing System (FOSS) has the potential to replace conventional instrumentation for strain, temperature, structural shape, and cryogenic liquid-level sensing. The first Optical Frequency Domain Reflectometry (OFDR)-based fiber-optic interrogation system has been successfully designed, fabricated, and tested under relevant launch environments. With successful environmental testing completed, a proto-qualified FOSS unit has passed all testing parameters and is ready to be integrated into a launch environment. These tests ensured confidence that the FOSS unit, residing under the NASA Low-Earth Orbit Flight Test of an Inflatable Decelerator (LOFTID) project, would be successful upon deployment and prove to remain operational during the re-entry mission.

Acknowledgments

The authors thank the following people for their hard work during this project: Jennifer Arney NASA (LaRC), FOSS Test Lead - without her effort, these environmental tests would not have been possible. Thanks to the many people from the LSP who provided help: Jeff Williams NASA (KSC), Thermal Lead; James Kinney NASA (KSC), Structural Lead; Kelles Veneri NASA (KSC), Systems Lead. We also thank the environmental testing groups at NASA KSC, AFRC, and LaRC, specifically, Karen Estes NASA (AFRC) and Courtney Rollins NASA (LaRC). Thanks to Richard Knochelmann NASA (MSFC) for the initial design of the FOSS enclosure, John Del Frate NASA (AFRC), and Eric Miller NASA (AFRC), FOSS Project Manager for their direction. Thank you to Lance Richards for his continued support in getting this project to where it is today. Thank you to everyone that was able to work continuously during the COVID pandemic, the experience was surreal, and to the many people from the FOSS group that supported all aspects of testing: Philip Harmony, Frank Peña, John Rudy, Daniel Budolak, Jackson Winter. and many others.

References

[1] Parker, Jr., A. R., Chan, H. M., Lopez-Zepeda, J., Pena, F, Swanson, G. T., Hughes, S., and Schallhorn, P., "Fiber Optics Sensing System deployment on Low-Earth Orbit Flight Test of an Inflatable Decelerator," AIAA SciTech 2024, (to be published).

[2] Prosser, W. H., Wu, M. C., Allison, S. G., DeHaven, S. L., and Ghoshal, A., "Structural Health Monitoring Sensor Development at NASA Langley Research Center," *Proceedings, Int. Conf. Computational & Experimental Engineering and Sciences* (ICCES) (Corfu, Greece), July 2003.

[3] Wu, Meng-Chou, Winfree, William P., and Allison, Sidney G., "Fiber Optics Thermal Health Monitoring of Aerospace Structures and Materials," paper 7294-42, *SPIE Smart Structures/NDE 2009*, (San Diego, California), March 9-12, 2009.

[4] Jutte, C. V., Ko, W. L., Stephens, C. A., Bakalyar, J. A., Richards, W. L., and Parker, A. R., *Deformed Shape Calculation of a Full-Scale Wing Using Fiber Optic Strain Data from a Ground Loads Test*, NASA/TP-2011-215975, December 2011.

[5] Bakalyar, J., and Jutte, C., "Validation Tests of Fiber Optic Strain-Based Operational Shape and Load Measurements," AIAA Paper 2012-1904, April 2012.

[6] Johnson, Wesley L., Grotenrath, Ryan J., Balasubramaniam, Ramaswamy, Chan, Hon Mon, Smith, James W., and Giddens, Patrick, "Cryogenic Fluid In-Situ Liquefaction for Landers: Prototype Demonstration," AIAA ASCEND 2023, AIAA Paper 2023-4748, October 2023.

[7] Chan, H. M., *Novel Fiber Optic Sensing Arrays with Enhanced Sensitivity in Cryogenic Temperatures*, NASA/TM-20205009645, August 2021.

[8] Froggatt, M., and Moore, J., "Distributed measurement of static strain in an optical fiber with multiple Bragg gratings at nominally equal wavelengths," Applied Optics, Vol. 37, Issue 10, pp. 1741-1746, 1998.

[9] Richards, W. Lance, Parker, Jr., Allen R., Ko, William L., Piazza, Anthony, and Chan, Patrick, "Application of Fiber Optic Instrumentation," NATO RTO-AG-160, Vol. 22, SCI-228, July 2012.